$$C = \mu + \frac{(1-\mu)\left[\left(S_{13}^{II} + \frac{\mu S_{13}^{av}}{1-\mu}\right)S_{13}^{II} - \left(S_{11}^{II} + \frac{\mu S_{13}^{av}}{1-\mu}\right)S_{33}^{II}\right]}{\left(S_{13}^{II} + \frac{\mu S_{13}^{av}}{1-\mu}\right)S_{13}^{av} - \left(S_{11}^{II} + \frac{\mu S_{13}^{av}}{1-\mu}\right)S_{33}^{av}} \quad \text{(A18)}$$

$$D = \frac{(1-\mu)\left[\left(S_{11}^{II} + \frac{\mu S_{11}^{av}}{1-\mu}\right)(\alpha_{33}^{av} - \alpha_{33}^{I}) - \left(S_{13}^{II} + \frac{\mu S_{13}^{av}}{1-\mu}\right)(\alpha_{11}^{av} - \alpha_{11}^{II})\right]}{\left(S_{13}^{II} + \frac{\mu S_{13}^{av}}{1-\mu}\right)S_{13}^{av} - \left(S_{11}^{II} + \frac{\mu S_{13}^{av}}{1-\mu}\right)S_{33}^{av}} \quad \text{(A19)}$$

$$A = \frac{\left(S_{13}^{I} + \frac{\mu}{1-\mu}S_{13}^{av}\right)S_{13}^{I} - \left(S_{11}^{I} + \frac{\mu}{1-\mu}S_{11}^{av}\right)S_{33}^{I}}{\left(S_{13}^{I} + \frac{\mu}{1-\mu}S_{13}^{av}\right)S_{13}^{av} - \left(S_{11}^{I} + \frac{\mu}{1-\mu}S_{11}^{av}\right)S_{33}^{av}} \quad \text{(A20)}$$

$$B = \frac{(\alpha_{33}^{av} - \alpha_{33}^{I})\left(S_{11}^{I} + \frac{\mu}{1-\mu}S_{11}^{av}\right) - (\alpha_{11}^{av} - \alpha_{11}^{I})\left(S_{13}^{I} + \frac{\mu}{1-\mu}S_{13}^{av}\right)}{\left(S_{13}^{I} + \frac{\mu}{1-\mu}S_{13}^{av}\right)S_{13}^{av} - \left(S_{11}^{I} + \frac{\mu}{1-\mu}S_{11}^{av}\right)S_{33}^{av}} \quad \text{(A21)}$$

References and Notes

(1) Sakurada, I.; Nukushina, Y.; Ito, T. *J. Polym. Sci.* **1962**, *57*, 651.

(2) Sakurada, I.; Ito, T.; Nakamae, K. *Macromol. Chem.* **1964**, *75*, 1.

(3) Sakurada, I.; Kaji, K. *J. Polym. Sci., Part C: Polym. Symp.* **1970**, *31*, 57.

(4) Matsuo, M.; Sawatari, C. *Macromolecules* **1986**, *19*, 2036.

(5) Sawatari, C.; Matsuo, M. *Macromolecules* **1986**, *19*, 2653.

(6) Sawatari, C.; Matsuo, M. *Macromolecules* **1986**, *19*, 2726.

(7) Matsuo, M.; Sawatari, C.; Iwai, Y.; Ozaki, F. *Macromolecules.* Following paper in this issue.

(8) Matsuo, M.; Sato, R. In preparation.

(9) Hibi, S.; Maeda, M.; Makino, S.; Nomura, S.; Kawai, H. *Sen-i-Gakkaishi* **1973**, *29*, 79.

(10) Maeda, M.; Hibi, S.; Itoh, F.; Nomura, S.; Kawaguchi, T.; Kawai, H. *J. Polym. Sci., Polym. Phys. Ed.* **1970**, *8*, 1303.

(11) Takayanagi, M.; Imada, K.; Kajiyama, T. *J. Polym. Sci., Part C: Polym. Symp.* **1966**, *15*, 263.

(12) Roe, R. J.; Krigbaum, W. R. *J. Chem. Phys.* **1964**, *40*, 2608.

(13) Krigbaum, W. R.; Roe, R. J. *J. Chem. Phys.* **1964**, *41*, 737.

Effect of Orientation Distribution and Crystallinity on the Measurement by X-ray Diffraction of the Crystal Lattice Moduli of Cellulose I and II

Masaru Matsuo,* Chie Sawatari,† Yuki Iwai, and Fumihiko Ozaki‡

Department of Clothing Science, Faculty of Home Economics, Nara Women's University, Nara 630, Japan

Received June 23, 1989

ABSTRACT: The crystal lattice moduli of cellulose I and II were measured by X-ray diffraction using ramie and mercerized ramie. The measured crystal lattice moduli were in the range from 120 to 135 GPa and from 106 to 112 GPa for cellulose I and II, respectively. These values were different from recent theoretical estimates of 167 and 163 GPa for cellulose I and II, respectively, reported by Tashiro and Kobayashi. To study the origin of this difference, a numerical calculation of the crystal lattice modulus, as measured by X-ray diffraction, was carried out by considering effects of the orientation factors of crystal and amorphous chains and crystallinity. In this calculation, a previously introduced model was employed, in which oriented crystalline layers are surrounded by oriented amorphous phases and the strains of the two phases at the boundary are identical. The theoretical results indicate that the crystal lattice modulus measured by X-ray diffraction is different from the intrinsic lattice modulus when a parallel coupling between amorphous and crystalline phases is predominant, while the values of both moduli are almost equal when a series coupling is predominant. Thus, the crystal lattice moduli of cellulose I and II measured by X-ray diffraction are predicted to be dependent upon the morphological properties of the bulk specimens. The numerical calculations, however, indicate that the morphological dependence is less pronounced with increasing degree of molecular orientation and crystallinity. Thus, it is concluded that fibers and films with a high degree of molecular orientation and a high crystallinity should be used as test specimens for measuring crystal lattice moduli by X-ray diffraction.

I. Introduction

In previous papers, the crystal lattice moduli of polyethylene[1] and isotactic polypropylene[2] were studied by X-ray diffraction using ultradrawn specimens. The results obtained suggest that the stress in a ultradrawn specimen is almost equal to the external applied stress and that the homogeneous stress hypothesis commonly used to derive the crystal lattice modulus from X-ray measurement is valid. In related work,[3] a mathematical representation based on a linear elastic theory was proposed to account for the dependence of the measured crystal lattice modulus in the chain direction on molecular orientation and crystallinity.[3] This description indicated that the crystal lattice modulus as measured by X-ray diffraction is different from the intrinsic crystal lattice modulus, but the calculated value is almost independent of the molecular orientation and crystallinity, except in the case of a low degree of molecular orientation and low crystallinity.

* To whom all correspondence should be addressed.
† Faculty of Education, Shizuoka University, Shizuoka 442, Japan.
‡ Department of Polymer Material Engineering, Faculty of Engineering, Yamagata University, Yonezawa 992, Japan.

0024-9297/90/2223-3266$02.50/0

The question arises, however, whether or not the crystal lattice modulus measured by X-ray diffraction is equal to the intrinsic crystal modulus, if derived from measurements on a specimen with a low degree of molecular orientation and low crystallinity. Furthermore, it is important to consider whether the conformation and packing mode of chains within a crystal unit cell are important factors in the determination of the crystal lattice modulus. Cellulose samples provide suitable materials to pursue this problem, since there exist two kinds of stable crystal unit cells, cellulose I and II.

The structures of cellulose I and II were reported by Blackwell et al.[4,5] According to these authors, cellulose I consists of a crystalline array of parallel chains, and the unit cell is monoclinic with dimensions a = 16.34 Å, b = 15.72 Å, c = 10.38 Å (fiber axis), and γ = 97.0° with disaccharide segments of eight chains, the space group being $P2_1$. By contrast, the structure of cellulose II is comprised of an array of antiparallel chain molecules, and the unit cell is monoclinic with dimensions a = 8.01 Å, b = 9.04 Å, c = 10.36 Å (fiber axis), and γ = 117.1°, the space group being $P2_1$.

On the basis of the structures of cellulose I and II,[4,5] Tashiro and Kobayashi have calculated elastic compliances taking into consideration intramolecular and intermolecular hydrogen bonds.[6] The calculation was carried out by using the **B** matrix in the normal coordinate treatments to save a great amount of computer memory in the determination of the complicated crystal structure. They concluded that the crystal lattice moduli parallel to the crystal fiber axis of cellulose I and II are 167 and 162 GPa, respectively. This indicates that the crystal lattice modulus of cellulose I is almost equal to that of cellulose II, and the crystal modulus is determined principally by the chemical structure of a molecule and is independent of the detailed packing of the molecules. This result is different from the experimental results reported by Sakurada et al.[7] Their crystal lattice moduli of cellulose I and II are 130 and 90 GPa, respectively.

In order to address this discrepancy, measurements of the crystal lattice moduli of cellulose I and II were carried out by X-ray diffraction, using ramie and ramie mercerized with sodium hydroxide. The values measured are discussed in relation to molecular orientation and crystallinity by using a theoretical model discussed in the preceding paper in this issue.[8] The results are also compared with the values calculated by Tashiro and Kobayashi[6] to examine the dependence of morphological properties on the crystal lattice modulus measured by X-ray diffraction. First, the orientation factors F_{l0n} ($2 \le l \le 4$ and $0 \le n \le 4$) and G_{l0n} ($2 \le l, n \le 4$) of crystallites are estimated from the orientation distribution functions of the reciprocal lattice vectors of crystal planes by the method of Roe and Krigbaum;[9-11] the orientation factors F_{l00}^{am} ($2 \le l \le 4$) of amorphous chain segments are estimated by subtracting the crystalline contributions from the total birefringence. Second, the crystal lattice modulus measured by X-ray diffraction is calculated by using the values of F_{l0n}, G_{l0n}, and F_{l00}^{am}, according to a previously introduced theory.[8] A detailed analysis presents the importance of using fibers and films with a high degree of molecular orientation and a high crystallinity as test specimens for measuring crystal lattice moduli.

II. Experimental Section

1. Sample Preparation. Unconstrained ramie fibers were immersed into hot water containing 0.5% sodium hydroxide (NaOH) for 10 min to remove several kinds of resins, leached in running water for 5 h, and dried at ambient condition. The WAXD pattern of the specimen exhibited the typical diffraction characteristics from crystallites of cellulose I. Next, these fibers were kept at a constant length, immersed into hot water containing 20% NaOH for 1 h at 50 °C for mercerization, and then leached in running water for 3 days and dried at ambient condition. Through this process, cellulose I was transformed into cellulose II. The WAXD patterns do not exhibit the diffraction from crystalline alkali–cellulose complexes such as sodium cellulose I or sodium cellulose II in a sequence of apparently crystal–crystal phase transformations.[12,13]

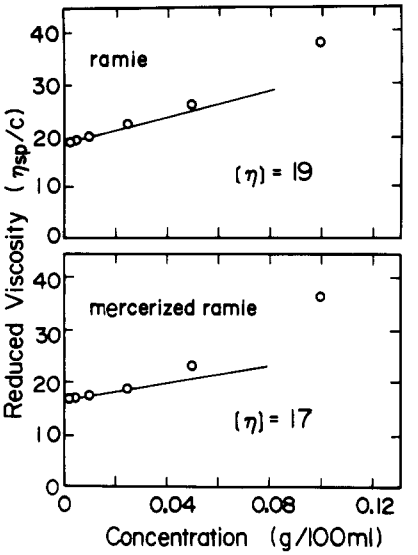

Figure 1. Relationship between reduced viscosity η_{sp}/c and concentration c.

2. Characterization of Test Specimens. Densities of the ramie and the mercerized ramie were measured with a pycnometer in nitrobenzene–carbon tetrachloride as a medium. Prior to measuring the density, the fibers were cut into fragments, immersed in an excess of ethanol for 1 week in an ultrasonic washing instrument, and subsequently vacuum dried for 3 days. The crystallinities of ramie and mercerized ramie were calculated by using 1.635[14] and 1.497[15] g·cm^{-3} for the intrinsic densities of the crystal and amorphous phases, respectively. The crystallinities of ramie and mercerized ramie were determined to be 56% and 35%, respectively.

The viscosity-average molecular weights of the ramie and the mercerized ramie were measured with an Ubbelohde-type capillary viscometer. For viscosity measurements, the dissolution was carried out by conversion from cellulose to methylcellulose using dimethyl sulfoxide and p-formaldehyde as solvents at 30 °C under nitrogen.[16] Figure 1 shows the results of these measurements, in which η_{sp} and c are the specific viscosity and the concentration of solution, respectively. The viscosity-average molecular weight $\bar{M}_v$ was calculated from the relationship $[\eta] = K\bar{M}^a$, assuming $K = 3.38 \times 10^{-2}$ and $a = 0.84$,[17] in which $[\eta]$ is defined by $\lim_{c \to 0} \eta_{sp}/c$. The values were 420 000 and 360 000 for cellulose I and II, respectively. This indicates that molecular degradation under the mercerization is not very significant, and both fibers can be employed as test specimens to study the difference of the crystal lattice moduli between cellulose I and II.

The orientation of crystallites was evaluated in terms of orientation distribution functions derived from X-ray diffraction intensity distributions. The orientation of amorphous chain segments was derived from birefringence data and was estimated by subtraction of the crystalline contribution from the total birefringence, assuming simple additivity proposed by Stein and Noris.[18]

III. Results and Discussion

1. Orientation Distribution Function of Crystallites within Ramie and Mercerized Ramie. Figure 2 shows the crystal structures of cellulose I and II, in which a Cartesian coordinate system $0\text{-}U_1U_2U_3$ was fixed in

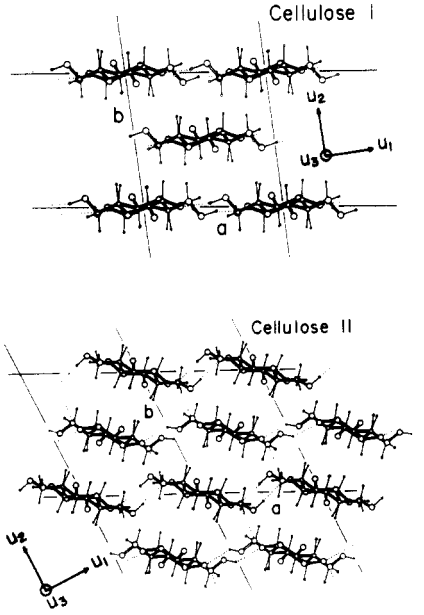

Figure 2. Crystal structures of cellulose I and II by Blackwell, in which the dotted line is the direction of hydrogen bonding.

such a way that the U_1, U_2, and U_3 axes are parallel to the reciprocal lattice vector of the (h00) plane, b-axis, and c-axis, respectively, so as to make the properties of this coordinate system orthorhombically symmetric. The orientation of a given vector $\mathbf{r}_j$ (reciprocal lattice vector of the jth crystal plane) is represented with respect to the polar and azimuthal angles Θ_j and Φ_j within the coordinate 0–$U_1U_2U_3$. Here we use the same notation as in the accompanying paper.[8]

The orientation distribution function of crystallites can be calculated on the basis of the orientation functions of the reciprocal lattice vectors measured by X-ray diffraction, applying the method proposed by Roe and Krigbaum.[9,10] The measurements of the X-ray diffraction intensity distribution were performed using an ordinary horizontal scanning type goniometer, operating at a fixed time step scan of 0.1° interval for a time of 20 s over a range of twice the Bragg angle, $2\theta_B$, from 9° to 53° by rotating about the film normal direction at 2~5° intervals from 0° to 90°.

The intensity distribution was measured as a function of $2\theta_B$ at a given rotational angle θ_j, and corrections were made for air scattering, background noise, polarization, absorption, incoherent scattering, and amorphous contributions. The intensity curve thus obtained was assumed to be due to the contribution of the intensity from the crystalline phase. The intensity curve $I_{cry}(2\theta_B)$ was separated into the contribution from the individual crystal planes assuming that each peak had a symmetric form given by a Lorentz function of $2\theta_B$ in eq 1, where I_j^0 is the maximum intensity of the jth peak

$$I_{cry}(2\theta_B) = \sum_j \frac{I_j^0}{1 + (2\theta_0^j - 2\theta_B)^2/(\beta_j)^2} \tag{1}$$

Here β is the half-width of the jth peak at half the peak intensity and θ_0^j is the Bragg angle at which the maximum intensity of the jth peak appears. By use of the same process at a given angle θ_j in the range from 0° to 90°, the intensity distribution $I_j(\theta_j)$ can be determined for the respective jth crystal plane, and the orientation distribution function of the jth reciprocal lattice vector may be given by

$$2\pi q_j(\cos\theta_j) = \frac{I_j(\theta_j)}{2\int_0^{\pi/2} I_j(\theta_j)\sin\theta_j\,d\theta_j} \tag{2}$$

Here it should be noted that there are some crystal planes whose Bragg angle reflections are located very close to each other. In this case, the function $g_j(\cos\theta_j)$ for the respective crystal planes cannot be represented because of the difficulty of peak separation. The composite function $q_j(\cos\theta_j)$ includes the contributions of several planes as follows:

$$2\pi q_j(\cos\theta_j) = 2\pi\sum_{i=1}^{N_j} C_{ji} q_{ji}(\cos\theta_j) \tag{3}$$

The concept underlying eq 3 was first presented by Roe and Krigbaum. N_j is the number of the jth superposed peaks, and C_{ji} is the relative (normalized) weight for the vector $\mathbf{r}_{ji}$. Before numerical calculation by computer; initial values of C_{ji} are given by

$$C_{ji} = F_{ji}/\sum_{i=1}^{N_j} F_{ji} \tag{4}$$

where F_{ji} is the structure factor of the jth crystal plane.

For a uniaxial system, the orientation distribution function $\omega(\cos\theta,\eta)$ of crystallites may be calculated from $2\pi q_j(\cos\theta_j)$ by a method proposed by Roe and Krigbaum:[9,10]

$$F_{l0}^j = \langle P_l(\cos\theta_j)\rangle = \int_0^{2\pi}\int_0^{\pi} q_j(\cos\theta_j)P_l(\cos\theta_j)\times \sin\theta_j\,d\theta_j\,d\phi_j \tag{5}$$

$$F_{l0}^j = F_{l00}\sum_i^{N_j} C_{ji}P_l(\cos\Theta_{ji}) + 2\sum_{n=2}^{l}\frac{(l-n)!}{(l+n)!}[F_{l0n}\sum_i^{N_j} C_{ji}\times P_l^n(\cos\Theta_{ji})\cos n\Phi_{ji} + G_{l0n}\sum_{i=1}^{N_i} C_{ji}P_l^n(\cos\Theta_{ji})\sin n\Phi_{ji}] \tag{6}$$

$$4\pi^2\omega(\cos\theta,\eta) = \frac{1}{2} + \sum_{l=2}^{\infty}\frac{(2l+1)}{2}\left[F_{l00}P_l(\cos\theta) + 2\sum_{n=2}^{l}\frac{(l-n)!}{(l+n)!}[F_{l0n}\cos n\eta + G_{l0n}\sin n\eta]P_l^n(\cos\theta)\right] \tag{7}$$

Here l and m are even integers; $P_l^n(x)$ and $P_l(x)$ are the associated Legendre polynomials. The coefficients F_{l0}^j, F_{l0n}, and G_{l0n} may be represented by the coefficients α_{l0}^j, A_{l0n}, and B_{l0n} given by Roe[11]

$$F_{l0}^j = \left(\frac{2}{2l+1}\right)^{1/2} 2\pi\alpha_{l0}^j \tag{8}$$

$$F_{l0n} = \left[\frac{2}{2l+1}\frac{(l+n)!}{(l-n)!}\right]^{1/2} 4\pi^2 A_{l0n} \tag{9}$$

$$G_{l0n} = \left[\frac{2}{2l+1}\frac{(l+n)!}{(l-n)!}\right]^{1/2} 4\pi^2 B_{l0n} \tag{10}$$

The coefficients F_{l0n} and G_{l0n} can be determined by solving the linear equations represented by eq 6, since there exist more equations than the number of unknowns, as was pointed out by Roe and Krigbaum.[9,10]

The values of weighting factors, ρ_i, required in the least-squares calculation, were assigned somewhat subjectively on the basis of the concept that the X-ray diffraction intensity is thought to be dependent upon the structure factor of each crystal plane. Hence, in this calculation, weight factors ρ_j as a first approximation were assumed

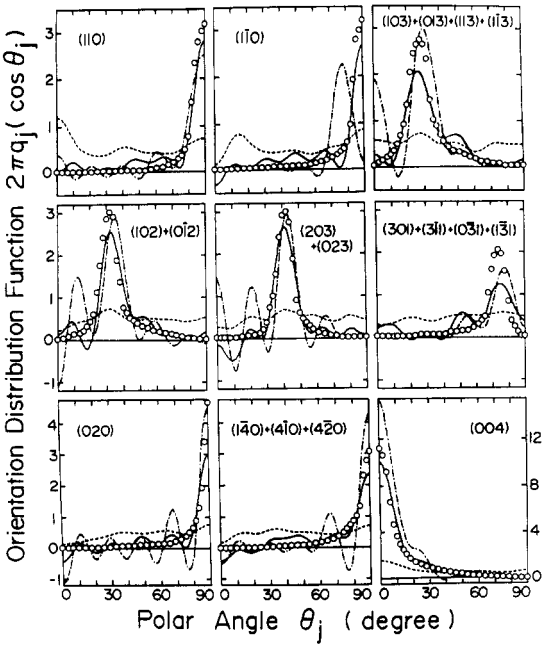

Figure 3. Orientation distribution functions $2\pi q_j(\cos\theta_j)$ of the reciprocal lattice vectors of the indicated crystal plane of ramie. Circles: values of $2\pi q_j$ ($\cos\theta_j$) obtained from experimental measurements. Solid curves: $2\pi q_j(\cos\theta_j)$ calculated with 19-term series (l up to 18) with the use of reconstructed F_{l0}^j value. Dotted curve: the same but with the use of F_{l0}^j value calculated from $\omega(\theta,\eta) > 0$. Dashed curve: the same but with the use of F_{l0}^j value calculated from $\omega(\theta,\eta) = 0$ at $\theta > 30°$.

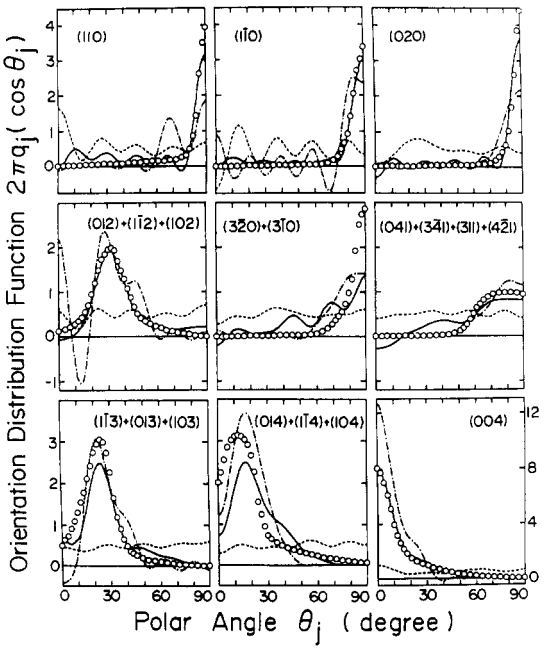

Figure 4. Orientation distribution functions $2\pi q_j(\cos\theta_j)$ of the reciprocal lattice vectors of the indicated crystal planes of mercerized ramie. Circle: values of $2\pi q_j(\cos\theta_j)$ obtained from experimental measurements. Solid curves: $2\pi q_j(\cos\theta_j)$ calculated with 19-term series (l up to 18) with the use of reconstructed F_{l0}^j value. Dotted curve: the same but with the use of F_{l0}^j value calculated from $\omega(\theta,c) > 0$. Dashed curve: the same but with the use of F_{l0}^j value calculated from $\omega(\theta,\eta) = 0$ at $\theta > 30°$.

to be almost proportional to the structure factor and were subsequently modified to obtain the best fit between experimental and calculated results through numerical calculations by computer.

Following Roe and Krigbaum,[9,10] the values of F_{l0n} and G_{l0n} were determined by the least-squares method. In doing so, the value of C_{ji} was determined by the simplex method, which is a direct search method to obtain the object function on the basis of trial and error.[19] The initial values of C_{ji} used in the simplex method were defined by eq 4, based on the structure factors F_{ji}. The calculation was continued until the best fit was achieved within the capability of the simplex method. By use of the final values of parameters, a mean square error between the calculated F_{l0}^j and recalculated F_{l0}^j was obtained

$$R = \frac{\sum_j \sum_l \rho_j [(F_{l0}^j)_{\mathrm{cal}} - (F_{l0}^j)_{\mathrm{recal}}]^2}{\sum_j \sum_l [(F_{l0}^j)_{\mathrm{cal}}]^2} \qquad (11)$$

Figures 3 and 4 compare the observed orientation distribution functions $2\pi q_j(\cos\theta_j)$ (open circles) with those (solid curve) recalculated for the respective crystal planes for the ramie and the mercerized ramie. We calculated the best values of F_{l0n} and G_{l0n} from eq 6 to minimize the value of R in eq 11. After that, we recalculated F_{l0}^j, in turn, from the values of F_{l0n} and G_{l0n} and further calculated $2\pi q_j(\cos\theta_j)$ from the recalculated F_{l0}^j value by using the following equation:

$$2\pi q_j(\cos\theta_j) = \frac{1}{2} + \sum_{l=2}^{\infty} \frac{(2l+1)}{2} F_{l0}^j P_l(\cos\theta_j) \qquad (12)$$

The values of R were calculated by using the values of C_{ji} and ρ_j to obtain the solid curves in Figures 3 and 4. They were 23.4% and 8.6%, for the ramie and the mercerized ramie, respectively.

Returning to Figures 3 and 4, it is evident that fairly good agreement between the observed and calculated distribution functions was obtained, even for the less accurately superposed crystal planes with lower weighting factors. The oscillations of the full curve are due to the procedure of expanding each sharp distribution function into an infinite series of spherical harmonics. This is an expected deficiency of this method. Actually, such oscillations shown in Figures 3 and 4 have never been observed for more common and less sensitive distribution functions $2\pi q_j(\cos\theta_j)$ used to investigate the deformation mechanism of polyethylene spherulites.[20]

Parts a and b of Figure 5 show the orientation distribution functions of crystallites $\omega(\cos\theta,\eta)$ calculated by using eq 7 with the coefficients F_{l0n} and G_{l0n} determined from eq 6 with l limited to 18. As can be seen from the figures, there exist several highly populated regions and negative regions that complicate the detailed analysis of the crystal transformation from cellulose I to cellulose II. Most of the regions appearing at wider angles of θ must be artifacts of expansion of the sharp experimental functions $2\pi q_j(\cos\theta_j)$ into infinite series of spherical harmonics. To demonstrate this, we employ two methods. As the first method, the orientation functions $2\pi q_j(\cos\theta_j)$ were recalculated from $\omega(\cos\theta,\eta)$ by assuming that negative regions in a and b of Figure 5 are zero. The calculation procedure is given by

$$F_{l0n} = \int_0^{2\pi}\int_0^{\pi} \omega(\cos\theta,\eta) P_l^n(\cos\theta) \cos n\eta \sin\theta \, d\theta \, d\eta \qquad (13)$$

$$G_{l0n} = \int_0^{2\pi}\int_0^{\pi} \omega(\cos\theta,\eta) P_l^n(\cos\theta) \sin n\eta \sin\theta \, d\theta \, d\eta \qquad (14)$$

$$F_{l0}^j = F_{l00} P_l(\cos\Theta_j) + 2\sum_{n=2}^{l} \frac{(l-n)!}{(l+n)!} [F_{l0n} \cos n\Phi_j + G_{l0n} \sin n\Phi_j] P_l^n(\cos\Theta_j) \qquad (15)$$

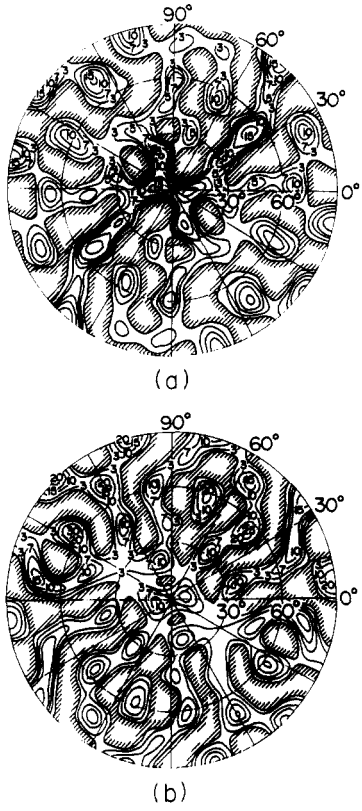

Figure 5. Orientation distribution functions of crystallites $\omega(\theta,\eta)$ calculated with 19-term series of expansion by eqs 5–7: (a) ramie; (b) mercerized ramie.

$$2\pi q_j(\cos\theta_j) = \frac{1}{2} + \sum_{l=2}^{\infty} \frac{(2l+1)}{2} F_{l0}{}^{j} P_l(\cos\theta_j) \qquad (16)$$

The dotted curves $q_j(\cos\theta_j)$ in Figures 3 and 4 show the results. All curves become smaller, and the calculated curves are in poor agreement with the observed results. Returning to Figure 5, it is seen that the complicated highly populated and negative regions appeared at θ larger than 30°. Judging from the profile of the distribution function of the reciprocal lattice vector of the (004) plane, it may be expected that the distribution functions $\omega(\cos\theta,\eta)$ do not have high dense populations at wider angles and become almost close to zero with increasing θ. On the basis of this concept, as the second method, the distribution function $\omega(\cos\theta,\eta)$ shown in parts a and b of Figure 6, corresponding to the enlargement of the profiles at $\theta \leq 30°$ in Figure 5a,b, is employed to recalculate $2\pi q_j(\cos\theta_j)$ by assuming that the distribution function $\omega(\cos\theta,\eta)$ at $\theta > 30°$ is zero. The dashed curves $q_j(\cos\theta_j)$ in Figures 3 and 4 show the orientation distribution of $2\pi q_j(\cos\theta_j)$ calculated on the basis of the second method. The calculated curves are in fairly good agreement with the experimental results. The result demonstrates that the highly populated and negative regions at $\theta > 30°$ in Figure 5 are artifacts as discussed before.

The two populations in the profiles in Figure 6 of $\omega(\cos\theta,\eta)$ in the range of η from 0° to 180° may be explained in terms of two types of preferential orientation of cellulose I and II crystallites. For cellulose I, the peaks appeared around $\theta = 9°$, $\eta = 175°$ and $\theta = 20°$, $\eta = 110°$, while for cellulose II the peaks were around $\theta = 8°$, $\eta = 15°$ and $\theta = 22°$, $\eta = 105°$; the maximum peak of the orientation distribution function of the c-axis appeared at $\theta_j = 0°$ as shown in Figures 3 and 4. Warwicker[21] pointed out that the spiral angles in the successive layers of ramie differ, those in the outer layers being generally greater than those in the inner layers. However, information concerning these spiral angles is scarce, and precise values are not available. According to Warwicker's view, the former populations in $\omega(\cos\theta,\eta)$ of the ramie and the mercerized ramie are related to the main spiral angle in the inner layers along the fiber axis; the latter are related to the main spiral angle in the outer layers. Interestingly, both the spiral angles of ramie are hardly affected by mercerization. According to the packing structures of cellulose chains, proposed by Blackwell et al.,[4,5] the former peaks for cellulose I and II are related to the intermolecular hydrogen bonds (shown by dotted lines in Figure 2), and the latter are probably related to the direction of high electron density within crystal units. On average, however, the distribution function of the c-axis, corresponding to the reciprocal lattice vector of the (004) plane, has only a maximum peak at $\theta_j = 0°$, which is indicative of the preferential orientation with respect to the fiber axis shown in Figure 2. Thus it appears that the profile of the orientation distribution function $\omega(\cos\theta,\eta)$ is not similar to that of the c-axis obtained by integration of $\omega(\cos\theta,\eta)$ by η in the range from 0° to 180°.

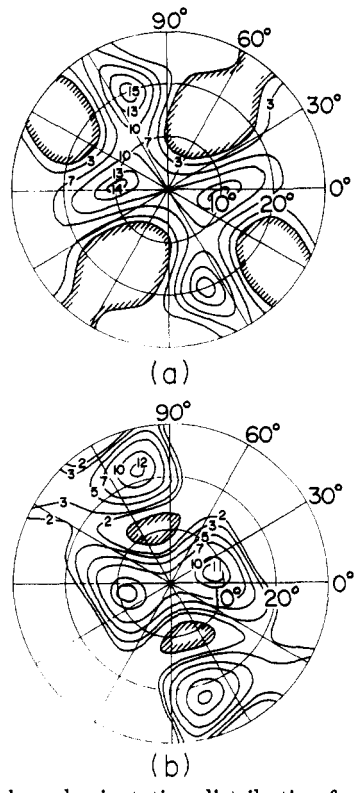

Figure 6. Enlarged orientation distribution function of crystallites $\omega(\theta,\eta)$ in the region $\theta \leq 30°$: (a) ramie; (b) mercerized ramie.

2. Orientation of Amorphous Chain Segments within Ramie and Mercerized Ramie. The contribution from the refractive index tensor n_{ij}^{c} of the crystallographic structural unit to the principal refractive tensor N_{ij}^{c} of bulk material is given by

$$\langle N_{ij}^{c} \rangle = \sum_{k=1}^{3} \sum_{l=1}^{3} n_{kl}^{c} \langle t_{ik} t_{jl} \rangle \qquad (17)$$

where t_{ik} is, for example, the direction cosine between the X_i axis and the V_k axis. n_{33}^{c}, n_{22}^{c}, and n_{11}^{c} are the refractive indexes along the U_3, U_2, and U_1 axes, respectively.

The contribution from the principal refractive index tensor n_{ij}^{c} of cellulose I (or cellulose II) to the refractive

index tensor n_{ij}^c is also given by

$$\langle n_{ij}^c \rangle = \sum_{k=1}^{3}\sum_{l=1}^{3} n_{kl}^{co} \langle m_{ik} m_{jl} \rangle \quad (18)$$

where m_{ik} is, for example, the direction cosine between the U_i axis and V_k axis, in which n_{33}^{co}, n_{22}^{co}, and n_{11}^{co} are the refractive indexes along the V_3 axis (chain axis), V_2 axis (normal to the pyranose ring), and V_1 axis (parallel to the pyranose ring). In the present case, the U_3 axis is equal to the V_3 axis, and eq 18 can be developed as a function of the angle Φ_0 between the U_1 and V_1 axes by assuming $n_{ij}^{co} = 0$ $(i \neq j)$. It is given by

$$\begin{aligned} n_{33}^c &= n_{33}^{co} \\ n_{22}^c &= n_{11}^{co} \sin^2 \Phi_0 + n_{22}^{co} \cos^2 \Phi_0 \\ n_{11}^c &= n_{11}^{co} \cos^2 \Phi_0 + n_{22}^{co} \sin^2 \Phi_0 \end{aligned} \quad (19)$$

The principal refractive indexes n_{33}^{co}, n_{22}^{co}, and n_{11}^{co} were calculated from the Lorentz–Lorenz relation by utilizing the values of bond polarizabilities proposed by Clement[22] and by neglecting the uncertain effect of the internal field within the crystal and of secondary bonds on the principal polarizabilities. Thus we have

$$\begin{aligned} n_{33}^{co} &= 1.6328 \\ n_{22}^{co} &= 1.4708 \\ n_{11}^{co} &= 1.6190 \end{aligned} \quad (20)$$

The angles Φ_0 for cellulose I and II crystal units are −7.0° and 29.33°, respectively.

In order to obtain the birefringence contribution Δ_c of crystallites, the mean value $\langle N_{ij}^c \rangle$ was calculated by taking the average of the orientation distribution function over all the orientations of the structural units. The result is

$$\begin{aligned} \Delta_c &= \langle N_{33}^c \rangle - \langle N_{22}^c \rangle \text{ (or } \langle N_{11}^c \rangle) \\ &= \left[n_{33}^c - \frac{1}{2}(n_{11}^c + n_{22}^c) \right] F_{200} + \frac{1}{4}(n_{11}^c - n_{22}^c) F_{202} \end{aligned} \quad (21)$$

Assuming that the birefringence effect of the amorphous phase, Δ_{am}, may be estimated by subtracting the crystalline contribution from the total birefringence, Δ_t, we obtain

$$\Delta_{am} = \frac{\Delta_t - X_c \Delta_c}{1 - X_c} \quad (22)$$

Here X_c is the degree of volume crystallinity and Δ_{am} is related to the orientation factor F_{200}^{am} as follows:

$$\Delta_{am} = \left[n_{33}^{am} - \frac{1}{2}(n_{11}^{am} + n_{22}^{am}) \right] F_{200}^{am} \quad (23)$$

The indices n_{33}^{am} and n_{11}^{am} $(=n_{22}^{am})$ for the amorphous chain segment were also estimated by the Lorentz–Lorenz equation and are 1.5863 and 1.5061, respectively. Here the pyranose ring was assumed to be a rotational ellipsoid around its chain axis. The value of F_{200}^{am} was 0.547 and and 0.488 for the ramie and the mercerized ramie, respectively.

To calculate the mechanical properties according to the method in the preceding paper,[8] the fourth moment orientation factor of the amorphous chain segments must be estimated. Unfortunately, this moment cannot be obtained from birefringence measurements and therefore must be calculated by assuming a common function. In this paper, the mean fourth power of direction cosine $\langle \cos^4 \theta \rangle$ was calculated from an inversely superposed Gaussian type function $G(\theta)$ as follows:

$$\langle \cos^4 \theta \rangle = \frac{\int_0^{\pi/2} G(\theta) \cos^4 \theta \sin \theta \, d\theta}{\int_0^{\pi/2} G(\theta) \sin \theta \, d\theta} \quad (24)$$

where

$$G(\theta) = \exp(-\theta^2/2\sigma^2) + \exp(-(\theta - \pi)^2/2\sigma^2) \quad (25)$$

The values of $\langle \cos^4 \theta \rangle$ can be obtained graphically from the experimental values of $\langle \cos^2 \theta \rangle$ for amorphous chain segments, since the relation of $\langle \cos^2 \theta \rangle$ versus $\langle \cos^4 \theta \rangle$ can be calculated by varying the parameter σ. Thus, the fourth-order orientation factor F_{400}^{am} can be obtained.[23]

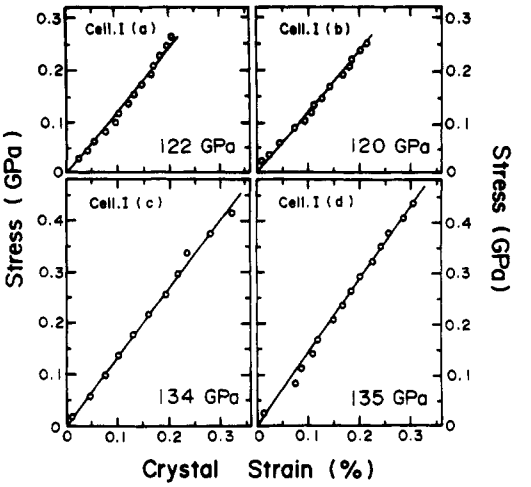

Figure 7. Stress–strain relationship for the crystal (004) plane of cellulose I.

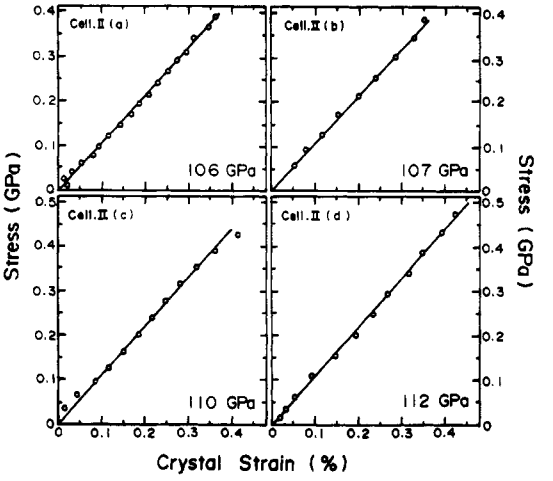

Figure 8. Stress–strain relationship for the crystal (004) plane of cellulose II.

3. Crystal Lattice Modulus of Cellulose I and II. Figures 7 and 8 show the relationship between the stress and the crystal lattice strain for cellulose I and II, respectively. The plots show a linear relationship in the given range of lattice strain. It should be noted that the crystal lattice modulus ranges from 120 to 135 GPa for cellulose I and from 106 to 112 GPa for cellulose II. This result indicates that the crystal lattice modulus of cellulose I is higher than that of cellulose II. The value for cellulose I is almost equal to that reported by Sakurada,[7] but that for cellulose II is higher. According to a recent theoretical study of Tashiro and Kobayashi, the elastic compliances of cellulose I and II are given as follows:[6]

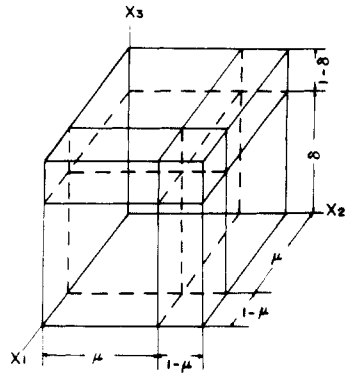

Figure 9. Composite model in which oriented crystallites are surrounded by an anisotropic amorphous phase.

Table I
Characteristics of Ramie and Mercerized Ramie

	ramie	mercerized ramie
crystallinity, %	56.0	34.7
the second-order orientation factor of the c-axis	0.718	0.714
the second-order orientation factor of amorphous chain segments	0.547	0.488
degree of polymerization	1900	1600
Young's modulus, GPa	26~29	23~24
tensile modulus, MPa	95~100	85~95
elongation at break point, %	2.44	2.34

For cellulose I

S_{ij} (10^{-2}/GPa) =

$$\begin{bmatrix} 1.990 & -0.839 & 0.029 & 0 & 0 & 2.210 \\ -0.839 & 9.400 & -0.054 & 0 & 0 & -9.530 \\ 0.029 & -0.054 & 0.597 & 0 & 0 & 0.005 \\ 0 & 0 & 0 & 30.529 & -5.416 & 0 \\ 0 & 0 & 0 & -5.416 & 13.351 & 0 \\ 2.210 & -9.530 & 0.005 & 0 & 0 & 32.698 \end{bmatrix} \quad (26)$$

For cellulose II

S_{ij} (10^{-2}/GPa) =

$$\begin{bmatrix} 5.836 & -1.427 & -0.021 & 0 & 0 & 1.036 \\ -1.427 & 6.684 & -0.005 & 0 & 0 & -4.628 \\ -0.021 & -0.005 & 0.617 & 0 & 0 & -0.008 \\ 0 & 0 & 0 & 48.620 & 36.864 & 0 \\ 0 & 0 & 0 & 36.864 & 46.946 & 0 \\ 1.036 & -4.628 & -0.008 & 0 & 0 & 21.773 \end{bmatrix} \quad (27)$$

From the value of S_{33} in eqs 26 and 27, the theoretical crystal lattice moduli were calculated to be 167 and 162 GPa for cellulose I and II, respectively. Interestingly, these calculations also show that the crystal lattice modulus of cellulose I is almost equal to that of cellulose II. This indicates that the crystal lattice modulus in the chain direction is hardly affected by interchain hydrogen bonding and is only dependent on the intrachain hydrogen bonding. Assuming that Tashiro and Kobayashi's calculations are correct, the difference between the experimental results of the crystal lattice moduli in Figures 7 and 8 and the theoretical lattice moduli must be due to the morphological structure of the ramie and the mercerized ramie.

The characteristics of ramie and mercerized ramie are summarized in Table I. As can be seen in this table, the second-order orientation factors and crystallinity are much lower than those typically found for ultradrawn polyethylene and polypropylene. Therefore, numerical calculation was carried out according to the mathematical description discussed in the preceding paper[8] that accounts for the effects of chain misalignment and amorphous material on the lattice modulus determined by X-ray diffraction. This theory is based on a model system shown in Figure 9, in which oriented crystalline layers are surrounded by an anisotropic amorphous plane, so that the strains of the two phases at the boundary in three directions are identical. At $\mu = 1$, this model corresponds to a series one, while at $\delta = 1$ it corresponds to a parallel one.[24]

The elastic compliances $S_{\mu\nu}^{ao}$ of the amorphous phase needed in the calculation are not precisely known. Following our crude approximation described elsewhere,[3] we estimated the elastic compliances S_{11}^{ao} and S_{22}^{ao} by double differentiation of Lennard-Jones potential energy functions, while the compliance S_{33}^{ao} was estimated assuming that the modulus along the chain axis is proportional to the number of molecular chains in the unit area perpendicular to the chain axis. Thus we have

$$S_{11}^{ao} = S_{22}^{ao} = (\rho_c/\rho_a)^4 S_{11}^{c'}$$
$$S_{33}^{ao} = (\rho_c/\rho_a) S_{33}^{c'} \quad (28)$$

where the compliances $S_{\mu\nu}^{c'}$ correspond to $S_{\mu\nu}^{cv}$ at $\theta = 0$

$$S_{11}^{c'} = \frac{1}{8}(3S_{11}^{co} + 3S_{22}^{co} + 2S_{12}^{co} + S_{66}^{co})$$
$$S_{33}^{c'} = S_{33}^{co} \quad (29)$$

According to Hibi et al.,[25] the other compliances can be estimated as

$$S_{44}^{ao} = S_{55}^{ao}$$
$$S_{12}^{ao} = -\nu_{21}^{ao} S_{11}^{ao}$$
$$S_{23}^{ao} = S_{13}^{ao} = -\nu_{31}^{ao} S_{33}^{ao}$$
$$2S_{11}^{ao} = (2S_{13}^{ao} + S_{55}^{ao})\Omega$$
$$2S_{11}^{ao} = 2S_{12}^{ao} + S_{66}^{ao} \quad (30)$$

where ν_{21}^{ao} and ν_{31}^{ao} are the Poisson ratios of the amorphous phase and both values are assumed to be equal in actual calculations. The parameter Ω was first introduced by Hibi et al.[25] to calculate the elastic compliance S_{55}^{ao} of oriented poly(vinyl alcohol) films. The value of Ω was in the range 0.7~1.0 for the best fit between the experimental and calculated value of Young's modulus.

Figure 10 shows the Poisson ratio dependence of Young's modulus E against Ω and δ (or μ), calculated for various crystallinities by using the second- and fourth-order orientation factors of crystal and amorphous phases of the ramie. As shown in this graph, Young's modulus E depends on Ω and δ (or μ) but is independent of the Poisson ratio.

Figure 11 displays the Poisson ratio dependence of the ratio E_c/E_c^0, in which E_c and E_c^0 correspond to the crystal lattice modulus measured by X-ray diffraction and the intrinsic crystal lattice modulus of cellulose I, respectively. The value of E_c^0 was taken to be 167 GPa calculated by Tashiro and Kobayashi, as discussed before.[6]

The results in Figures 10 and 11 indicate that the values of E and E_c/E_c^0 are independent of the Poisson ratio. The same tendency was obtained for cellulose II. Therefore, the Poisson ratio was taken to be 0.33 in the following calculations. The significant effect of Ω on E and E_c/E_c^0 is due to the fact that averaged elastic compli-

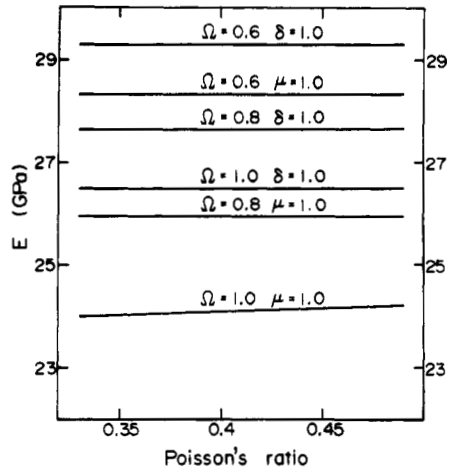

Figure 10. Poisson ratio dependence of Young's modulus E against Ω calculated for ramie.

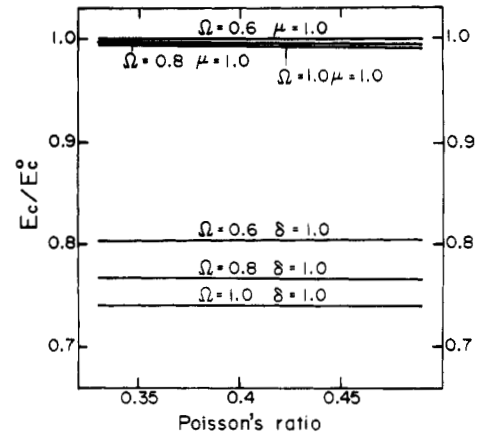

Figure 11. Poisson ratio dependence of the ratio E_c/E_c^0, in which E_c and E_c^0 correspond to the crystal lattice modulus measured by X-ray diffraction and the intrinsic crystal lattice modulus, respectively, for ramie.

ances S_{ij}^{av} are strongly affected by the value of S_{55}^{a0}, calculated from eq 30, as listed in Table II. Thus, it turns out that the shear modulus of the amorphous phase plays a more important role in the determination of Young's modulus in comparison with the Poisson ratios. This dependence becomes more pronounced at $\delta = 1$, which corresponds to a parallel model.

Figure 12 shows the δ dependence of Young's modulus E, calculated for the ramie and the mercerized ramie. This result indicates that E depends on the parameter Ω, which characterizes the elastic compliance S_{55}^{a0}, as has been reported for poly(vinyl alcohol) by Hibi et al.[25] At a constant value of Ω, E increases with δ. This result predicts that two specimens with the same crystallinity and degree of molecular orientation may have different Young's moduli, depending on the composite mode of crystalline and amorphous phases. The calculated results of the ramie (cellulose I) are in fairly good agreement with the experimental ones (26–29 GPa), with proper choice of the values of Ω and δ. But those for the mercerized ramie (cellulose II) are slightly lower than the experimental values (23–24 GPa).

Figure 13 shows the δ dependence of the ratio E_c/E_c^0 for three different values of Ω. For cellulose I, E_c/E_c^0 decreases with increasing δ, and this tendency is most significant at $\Omega = 1$. For cellulose II, the ratio shows nonlinear dependence with a peak whose position increases with decreasing Ω. Here the value of 162 GPa calculated by Tashiro and Kobayashi was used for E_c^0. The results indicate that the crystal lattice modulus of cellulose I measured by X-ray diffraction is estimated to be below the intrinsic values; this discrepancy becomes more pronounced as δ increases. By contrast, the measured value of cellulose II is estimated to exceed the intrinsic value at $\delta < 0.7$ in the case of $\Omega = 1.0$ and at $\delta < 0.88$ in the case of $\Omega = 0.8$; it is estimated to be lower in other cases. At $\mu = 1$, the crystal lattice moduli E_c measured by X-ray diffraction are almost equal to the intrinsic lattice moduli E_c^0. The main importance is whether the morphological properties of test specimens can be approximated with the series model. If the parallel approximation is more appropriate than the series model, the intrinsic values of the lattice modulus cannot be measured by the X-ray diffraction method.

According to our previous work,[8] one can avoid this problem by using test specimens with high crystallinity and high orientational degree of molecules. The mathematical model developed in the preceding paper[8] indicated that the crystal lattice modulus E_c, measured by X-ray diffraction, is equal to the intrinsic modulus E_c^0, if μ, δ, and F_{l00} are unity and F_{l0n} and G_{l0n} are zero. The values of the crystal lattice modulus measured by X-ray diffraction by several authors, however, were almost the same, within experimental error. This indicates that the morphological structure of the crystalline polymers used can be approximated by a series model. For example, the values for polyethylene and polypropylene by Sakurada et al.[7] were almost the same as those measured by using ultradrawn specimens.[1,2] The numerical calculations demonstrated that the crystal lattice modulus measured by X-ray diffraction approaches the intrinsic value when specimens with a crystallinity > 70% and the second-order orientation factor $F_{200} > 0.9$ are employed.

The theoretical values of the crystal lattice modulus have been generally in poor agreement with the experimental ones. Even for polyethylene, the theoretical value of 315 GPa by Tashiro et al.[26] is much higher than the experimental values of 215~235 GPa measured by X-ray diffraction.[1,7] This may be due to the difficulty in determining the real values of force constants of bonds. The theoretical values of the crystal moduli of cellulose I and II by Tashiro and Kobayashi[6] remain unresolved problems. However, on the basis of their values of elastic compliances, it turned out that the crystal lattice modulus measured by X-ray diffraction is dependent upon the morphological properties of a test specimen, and consequently fibers and/or films with a high degree of molecular orientation and high crystallinity must be used for measuring their crystal lattice moduli.

Judging from the above concept, it is very difficult to understand whether the morphological properties of the ramie and the mercerized ramie used in this experiment can be represented by a series model. This is based on the fact that the orientation factors and crystallinities of the specimens were lower than those of drawn polyethylene and polypropylene used by Sakurada et al.[7] Nevertheless, it is believable that the crystal lattice modulus of cellulose II obtained in this paper is close to the real value in comparison with the result of Sakurada et al.,[7] since the mercerized ramie used in this experiment has higher orientational degree of molecules than viscose rayon used by them. In order to obtain more conclusive answers for the morphological dependence of the crystal lattice modulus measured by X-ray diffraction, the experimental result shall be obtained as a function of the orientation factors of molecules and crystallinity using nylon 6 and poly(ethylene terephthalate).[27]

Table II
Intrinsic Elastic Compliance S_{55}^{ao} of Amorphous Phase and the Average Elastic Compliances S_{11}^{av}, S_{33}^{av}, S_{12}^{av}, and S_{13}^{av} of Amorphous Phase Obtained from the Indicated Value of Ω (/GPa)

	Ω for cellulose I			Ω for cellulose II		
	0.6	0.8	1.0	0.6	0.8	1.0
S_{55}^{ao}	0.1434	0.1898	0.2362	0.1215	0.1605	0.1995
S_{11}^{av}	0.1088	0.1110	0.1132	0.0904	0.0924	0.0944
S_{33}^{av}	0.0421	0.0491	0.0561	0.0397	0.0459	0.0521
S_{12}^{av}	−0.0274	−0.0283	−0.0291	−0.0219	−0.0228	−0.0237
S_{13}^{av}	−0.00811	−0.0116	−0.0151	−0.00760	−0.0107	−0.0138

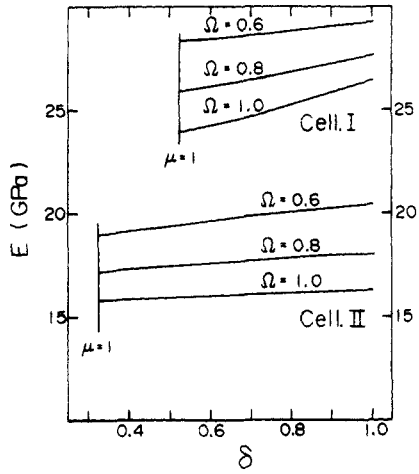

Figure 12. δ dependence of Young's modulus calculated for the ramie and the mercerized ramie.

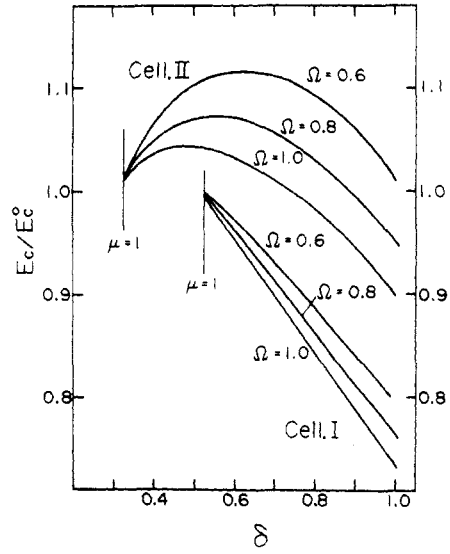

Figure 13. Ratio E_c/E_c^0 versus δ calculated for the ramie and the mercerized ramie.

IV. Conclusion

The crystal lattice moduli of cellulose I and II were measured by X-ray diffraction using ramie and mercerized ramie fibers, and these values were in the range 122–135 and 106–112 GPa for cellulose I and II, respectively. These values are different from the theoretical values by Tashiro and Kobayashi: 167 GPa for cellulose I and 162 GPa for cellulose II.[6] Theoretical calculations of the determination of the crystal lattice modulus by X-ray diffraction were carried out to investigate whether or not the homogeneous stress hypothesis is valid even in test specimens with a low degree of molecular orientation and low crystallinity such as ramie and mercerized ramie. The calculations were based on a model in which the oriented crystalline layers are surrounded by an anisotropic amorphous phase, and the strains of the two phases at boundaries are identical. The actual calculation was carried out by using theoretical intrinsic elastic compliances by Tashiro and Kobayashi and the orientation factors obtained from orientation distribution functions of the reciprocal lattice vectors of the given crystal planes by Roe and Krigbaum's method.[9-11] It was found that the crystal lattice modulus measured by X-ray diffraction is almost equal to the intrinsic crystal modulus if the morphology of the test specimen can be represented by a series model. By contrast, if a parallel model is more appropriate, the difference between the measured modulus and the intrinsic value can be pronounced. Furthermore, it turns out that the values of the orientation factor and crystallinity may cause significant effects on the value of the crystal lattice modulus derived from X-ray measurements. From a series of results, it may be concluded that the measurement of the crystal lattice modulus by X-ray diffraction must be carried out by using films and/or fibers with a high degree of molecular orientation and high crystallinity.

Acknowledgment. We thank Dr. K. Tashiro, Department of Polymer Science, Faculty of Science, Osaka University, for useful discussions, especially on his theory. We are indebted to Prof. P. Smith, Materials Department and Department of Chemical & Nuclear Engineering, University of California, Santa Barbara, for valuable discussions, comments, and suggestions in addition to his kind help with the English presentation.

References and Notes

(1) Matsuo, M.; Sawatari, C. *Macromolecules* **1986**, *19*, 2036.
(2) Sawatari, C.; Matsuo, M. *Macromolecules* **1986**, *19*, 2653.
(3) Sawatari, C.; Matsuo, M. *Macromolecules* **1986**, *19*, 2726.
(4) Gardner, K. H.; Blackwell, J. *Biopolymer* **1974**, *13*, 1975.
(5) Kolpak, F. J.; Blackwell, J. *Macromolecules* **1976**, *9*, 273.
(6) Tashiro, K.; Kobayashi, M. *Polymer Prepr. Jpn.* **1988**, *37*, 3017.
(7) Sakurada, I.; Kaji, K. *J. Polym. Sci., Part C: Polym. Symp.* **1970**, *31*, 57.
(8) Matsuo, M. *Macromolecules*. Submitted.
(9) Roe, R. J.; Krigbaum, W. R. *J. Chem. Phys.* **1964**, *40*, 2608.
(10) Krigbaum, W. R.; Roe, R. J. *J. Chem. Phys.* **1964**, *41*, 737.
(11) Roe, R. J. *J. Appl. Phys.* **1965**, *36*, 2024.
(12) Okano, T.; Sarko, A. *J. Appl. Polym. Sci.* **1984**, *29*, 4175.
(13) Okano, T.; Sarko, A. *J. Appl. Polym. Sci.* **1985**, *30*, 325.
(14) Treiber, E. *Die Chemie der Pflanzen zell ward*; Springer: Berlin, 1957.
(15) Hermans, P. H. *Physics and Chemistry of Cellulose Fiber, Part II*; Elsevier: New York, 1949; pp 163–317.
(16) Johnson, D. C.; Nicholson, M. D.; Haigh, F. C. *Appl. Polym. Symp.* **1976**, *28*, 931.
(17) Swenson, H. A. *Appl. Polym. Symp.* **1975**, *28*, 945.
(18) Stein, R. S.; Norris, F. H. *J. Polym. Sci.* **1956**, *21*, 381.
(19) Spendly, W.; Hext, G. R.; Himsworth, F. R. *Technometrics* **1962**, *4*, 441.
(20) Fujita, K.; Suehiro, S.; Nomura, S.; Kawai, H. *Polym. J.* **1982**, *14*, 545.
(21) Warwicker, J. O. *Cellulose and its derivatives: chemistry, biochemistry and applications*; Ellis Horwood Limited: West Sussex, England, 1985;
(22) Clement, C.; Botherel, P. C. *R. Acad. Sci. (Paris)* **1964**, *258*, 475.

(23) Nomura, S.; Kawabata, S.; Kawai, H.; Yamaguchi, Y.; Fukushima, A.; Takahara, H. *J. Polym. Sci.* **1969**, *A27*, 325.
(24) Takayanagi, M.; Imaba, K.; Kajiyama, T. *J. Polym. Sci., Part C: Polym. Symp.* **1966**, *15*, 263.
(25) Hibi, S.; Maeda, M.; Mizuno, M.; Nomura, S.; Kawai, H. *Sen-i-Gakkaishi* **1973**, *29*, 729.
(26) Tashiro, K.; Kobayashi, M.; Tadokoro, H. *Macromolecules* **1978**, *11*, 914.
(27) Matsuo, M. To be submitted.

Registry No. Cellulose, 9004-34-6.

Excimer Fluorescence as a Molecular Probe of Polymer Blend Miscibility. 9. Effects of Guest Concentration and Annealing in Blends of Poly(2-vinylnaphthalene) with Poly(cyclohexyl methacrylate)

William C. Tao and Curtis W. Frank*

Department of Chemical Engineering, Stanford University, Stanford, California 94305-5025

Received August 4, 1989

ABSTRACT: Excimer fluorescence from poly(2-vinylnaphthalene) (viscosity-average molecular weight of 17 000) was used to study the morphology of blends with poly(cyclohexyl methacrylate) prepared by solvent casting from toluene at 295 K and annealing at 413 K. A lattice model involving three-dimensional electronic excitation transport (EET) was used to interpret the ratio of excimer-to-monomer fluorescence, I_D/I_M, for P2VN concentration >60 wt %, while an intramolecular one-dimensional EET model was applied to P2VN concentration <25 wt %. Before annealing there is a much higher probability of formation of both intramolecular and intermolecular excimer-forming sites relative to the annealed blend. Furthermore, the blends with P2VN concentration below 70 wt % approach the equilibrium morphology characteristic of 413 K much faster than those with higher concentrations. A concave-downward curvature in I_D/I_M with increasing P2VN concentration indicates a phase-separated system, while a concave-upward curvature is found for miscible blends. A linear relationship between I_D/I_M and P2VN concentration can result for miscible blends when there are no intermolecular excimer-forming sites or for immiscible blends, when the volume fraction of the rich phase is much greater than that of the lean phase.

I. Introduction

Excimer fluorescence is an effective and sensitive morphological tool for the study of miscibility of an aromatic vinyl polymer with a nonfluorescent host polymer.[1-16] A convenient measure of the degree of mixing at the molecular level is the photostationary excimer-to-monomer fluorescence ratio, I_D/I_M. One problem with establishing excimer fluorescence as a quantitative tool, however, is that there are two photophysical effects that are difficult to separate: the population of traps and the mode by which these traps are sampled. In general, each pendant aromatic chromophore can absorb unpolarized light, and the excitation energy can migrate among the ensemble of chromophores before eventually undergoing nonradiative or radiative decay from a pendant chromophore or lower energy excimer trap.[17] The difficulties in the interpretation of changes in I_D/I_M with respect to blend thermodynamics stem from the existence of several types of excimer-forming sites (EFS) and the complex pathway of electronic excitation transport (EET) leading to excimer fluorescence. The degree of chain coiling and the extent of guest polymer aggregation will influence both the EFS population and the EET mode by which these traps are sampled. An understanding of the coupled interaction between the number and types of EFS traps and the nature of the excitation transport process is essential to being able to describe the chain structure and the blend morphology.

Our objective is to establish a quantitative understanding of the photophysical properties of the blend of poly(2-vinylnaphthalene) (P2VN) with poly(cyclohexyl methacrylate) (PCMA). To set the stage for this study, we first review the highlights of previous photophysical work on polymer blends and related systems. Initial photophysical work was phenomenological and was based on the simple assumption that the observed I_D/I_M was proportional to the local concentration of aromatic rings. Phase separation was thus expected to lead to an increase in I_D/I_M. Experiments were designed based upon the predictions of equilibrium Flory–Huggins thermodynamics.[18]

The first group of experiments by several investigators on relatively high molecular weight polymers emphasized enthalpic contributions to the free energy of mixing. Gashgari and Frank[4-6,9] investigated low-concentration (0.2 wt %) blends of P2VN in a homologous series of poly(alkyl methacrylates) and observed I_D/I_M to pass through a minimum when the guest and host solubility parameters were equal. Similar results were found for poly(acenaphthylene) and poly(4-vinylbiphenyl) dispersed in the same homologous host matrix series. In addition, Soutar[19] observed a minimum in I_D/I_M as a function of solvent solubility parameter for poly(1-vinylnaphthalene) and poly(1-vinylnaphthalene-*co*-methyl methacrylate) in toluene/methanol and toluene/cyclohexane mixed solvent systems. A solvent series was also used by Li et al.[20] to examine I_D/I_M for polystyrene (PS) labeled with pyrene groups at regularly spaced intervals. In each of these cases, the value of the solubility

0024-9297/90/2223-3275$02.50/0